Charge density analysis of two polymorphs of antimony(III) oxide

Andrew E. Whitten,[a] Birger Dittrich,[b] Mark A. Spackman,*[a] Peter Turner[c] and Trevor C. Brown[a]

[a] *Chemistry, University of New England, Armidale, NSW, 2351, Australia.*
   E-mail: mspackma@une.edu.au
[b] *Institut für Kristallographie, Freie Universität Berlin, Takustr. 6, D-14195 Berlin, Germany*
[c] *Crystal Structure Analysis Facility, University of Sydney, NSW, 2006, Australia*

High-resolution X-ray diffraction data have been collected on the cubic polymorph of antimony(III) oxide (senarmontite) to determine the charge distribution in the crystal. The results are in quantitative agreement with crystal Hartree–Fock calculations for this polymorph, and have been compared with theoretical calculations on the orthorhombic polymorph (valentinite). Information about the nature of bonding and relative bond strengths in the two polymorphs has been extracted in a straightforward manner *via* topological analysis of the electron density. All the close contacts in both polymorphs are found to be similar in nature based on the value of the Laplacian, the magnitude of the electron density and the local energy density at the bond critical points, and these characterise the observed interactions as substantially polar covalent, similar to molecular calculation results on Si–O and Ge–O. Electrostatic potential isosurfaces reveal the octopolar nature of this function for senarmontite, and shed light on the observed packing arrangement of Sb_4O_6 molecules in the crystal.

Introduction

Antimony compounds combined with halides have long been known to retard the propagation of flames. Historically senarmontite, the cubic polymorph of antimony trioxide, has been used as an additive in various products such as plastics, while the other polymorph, valentinite, is of little commercial value. Changing the reaction conditions can produce varying proportions of either polymorph, and we anticipate that information on bonding in each of the polymorphs may assist in understanding the reasons for the preferential formation of a given polymorph in certain conditions. This paper reports the results of charge density investigations of the two polymorphs.

   Although charge density analysis is now an established subfield of crystallography, the number of studies carried out on compounds containing relatively heavy atoms remains rather small. Challenging problems often faced in the data analysis of such systems include large absorption, extinction and anomalous dispersion effects, and the possibilities of anharmonic thermal motion and anisotropic extinction. In addition, the low ratio of valence to core electrons in these compounds makes it difficult to study bonding features in the crystal, as the contribution to structure factors from core electrons tends to swamp the signal from valence electrons, except at low values of $\sin\theta/\lambda$. However, it is in precisely this region of reciprocal space that the attenuating effect of extinction on the observed intensities is the greatest. Corrections can be made for the problems mentioned here, but they nevertheless have the potential to compromise the charge density analysis, so care has to be taken and these limitations recognised when analysing the data. It is possible to minimise some of these effects by the use of very high-energy synchrotron radiation, as demonstrated by recent studies on stishovite (SiO_2), cuprite (Cu_2O) and $YBa_2Cu_3O_{6.98}$,[1] although this is not yet a routine solution. Problems associated with thermal motion can also be minimised by conducting the experiments at ultra-low temperatures, but in minerals such as those being studied presently, thermal motion is generally sufficiently reduced at moderately low temperatures.

   An increasingly common method of analysing experimental and theoretical electron densities is *via* the topology of the electron density, derived from the "atoms in molecules" theory of Bader.[2] As remarked by one of us in a recent review of the literature,[3] this type of analysis is becoming the *de facto* standard in the field, especially applied to high-quality X-ray data. The topological analysis differs from the traditional deformation density, which is a representation of the way in which the electron density is distorted from that of a superposition of spherical atoms due to the effects of bonding. The latter method does not provide quantitative details about bonding, whereas topological analysis of the electron density allows straightforward extraction of this type of information. This type of analysis is important in the present study as quantitative information regarding the bonding in these two polymorphs is expected to provide an indication of how the interactions in the crystal might relate to the different reactivities of the two polymorphs.

Experimental

Crystallography and X-ray data collection

Suitable crystals of senarmontite were prepared by sublimation of senarmontite powder at 600 °C under a nitrogen atmosphere in a Pyrex sublimation vessel.[4] Yields from the sublimation method were low and crystals of suitable size were only collected after repeating the process many times, each for periods of 5–7 days. Preliminary diffraction experiments showed that most crystals were affected by twinning and possessed high mosaicity, but extensive searching eventually yielded a suitable specimen on which the data was later collected.[5]

   Data collection was undertaken at the University of Sydney on a Bruker SMART 1000 CCD X-ray diffractometer. The crystal was attached with *Exxon Paratone N* to a short length of fibre supported on a thin piece of wire inserted in a steel mounting pin. The crystals were then quenched in a cold nitrogen gas stream from an Oxford Cryosystems Cryostream, while X-rays were produced from graphite monochromated, Mo-Kα radiation, generated from a sealed tube. Data collection was undertaken in three spheres with the camera at 30, 65 and 102° in 2θ and 4.0 cm from the sample. Each sphere was collected using ω scan increments of 0.2°, and with the ϕ axis at 0, 120°, for the first sphere, 30, 150, 270° for the second and 90, 210 and 330° for the third. Exposure times were 10, 15 and 20 s, respectively, for each of the three camera positions. The first 50 frames of

each sphere were recollected at the completion of the sphere to assess decay, and based on these frames it was evident that it was not a significant effect. Data for each sphere were integrated separately with SAINT[6] before concatenating for a Gaussian absorption correction with XPREP[6] and then scaling and merging with SORTAV.[7] Subsequent calculations were also performed using teXsan,[8] WinGX[9] and XSHELL[10] graphical user interfaces.

The structure of senarmontite was solved in the space group $Fd\bar{3}m$, (origin at $\bar{3}m$) by direct methods with SHELXS-97,[11] then extended and refined with SHELXL-97.[12] All atoms in the asymmetric unit were modelled with anisotropic displacement parameters (Fig. 1) and extinction was included in the refinements. The thermal and positional parameters obtained from the least squares refinement using SHELXL were used as starting values for the multipole refinement. Full crystallographic details are provided in Table 1.
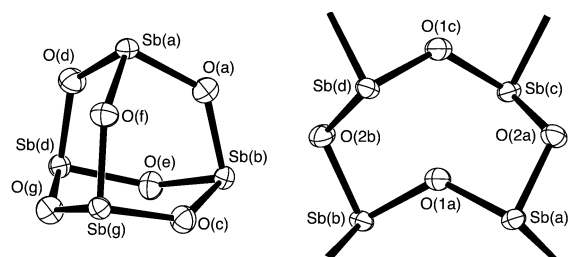

Fig. 1 Left: ORTEP[13] depiction (99% probability ellipsoids) of the Sb_4O_6 molecular moiety of senarmontite; letters in parentheses denote symmetry operations: (a) x, y, z; (b) $+x, 1/4 - y, 1/4 - z$; (c) $1/4 - z$, $1/2 + x, 3/4 - y$; (d) $z, 3/4 - x, 3/4 - y$; (e) z, y, x; (f) $1/4 - z, +y, 1/4 - x$ (g) $1/4 - x, 3/4 - z, y - 1/2$. Right: ORTEP depiction of two Sb_2O_3 chain links in the polymeric structure of valentinite; symmetry operations: (a) x, y, z; (b) $1/2 - x, 1/2 - y, z$; (c) $1/2 - x, y, z - 1/2$; (d) $x, 1/2 - y, z - 1/2$.

CCDC reference numbers 221438 and 223771.

See http://www.rsc.org/suppdata/dt/b3/b312550e/ for crystallographic data in CIF or other electronic format.

Charge density analysis

The rigid pseudoatom model for multipole refinement with X-ray diffraction data is well established, and a detailed description can be found in Coppens' recent book,[16] or Appendix A of the work by Flensburg et al.[17] VALRAY98[18] was used for the multipole refinements as well as subsequent mapping of properties and topological analyses. The multipole expansion extended up to the octopole[19] level on both antimony and oxygen atoms, while expansion-contraction parameters of the valence monopoles on all atoms were refined; apart from satisfying the atomic site symmetries, no additional symmetry was imposed on any of the peudoatoms. Core and spherical valence electron densities of the atoms were constructed from Clementi–Roetti atomic wavefunctions.[14] All other radial functions were of single exponential form, $r^n \exp(-ar)$ with $n = 8,8,8$ (dipole through octopole) for antimony atoms and $n = 2,2,3$ for oxygen atoms; radial exponents, a, were initially set at standard values of 8.40 au for antimony and 4.47 au for oxygen. Charge transfer was allowed between the antimony and oxygen atoms, and anisotropic displacement parameters were refined on all atoms. For antimony anharmonic displacement parameters were also refined, described by a Gram–Charlier expansion up to fourth order. No correlations were observed between thermal parameters and multipole populations (although some fourth-order anharmonic terms correlate with harmonic displacement parameters) and it is seen (Table 2) that although the values are small, the significance of these anharmonic parameters is generally high and they have a large influence on the final residuals. An isotropic extinction correction (type II[20]) was also included (the largest correction was 0.624 on F), and the refinement was

Table 1 Crystallographic data for senarmontite

Crystal data

Chemical formula	Sb_2O_3
Chemical formula weight	291.50
Space group	Cubic, $Fd\bar{3}m$ (no. 227)
$a, b, c/\text{Å}$	11.1160(4)
$V/\text{Å}^3$	1373.55(9)
$F(000)$	2016
Z	16
$D_c/\text{g cm}^{-3}$	5.638
Radiation type	Mo-Kα
$\lambda/\text{Å}$	0.71073
No. of reflections for cell parameters	5940
μ/mm^{-1}	15.536
T/K	100(2)
Crystal form	Truncated octahedron
Crystal size/mm	0.24 × 0.30 × 0.19
Crystal colour	Colourless

Data collection

Diffractometer	Bruker SMART 1000 CCD
Absorption correction	Gaussian
T_{min}	0.0624
T_{max}	0.2383
No. of measured reflections	20495
No. of observed reflections	629
Criteria for observed reflections	$I > 2\sigma(I)$
R_{int}	0.0320
$\theta_{max}/°$	65.56
Range of hkl	−26 to 28, −25 to 26, −24 to 28
Completeness (%)	99.8
Redundancy (average)	29.0

Multipole refinement details

Refinement on	F^2
Highest multipole	Octopole
$R(F)$	0.0130
$R_w(F^2 > 3\sigma(F_o^2))$	0.0431
S	3.72
Reflections used in refinement	629
Parameters used	27
Weighting scheme	$1/\sigma^2(F^2)$
Extinction method	Type II, isotropic, Gaussian distribution
Extinction coefficient $\rho/\text{Å}$	1.27(4) × 10^3
Source of atomic scattering factors	Calculated in VALRAY using atomic wavefunctions[14]
Dispersion corrections[15]	$f'(\text{Sb}) = -0.587, f''(\text{Sb}) = 1.546$, $f'(\text{O}) = 0.011, f''(\text{O}) = 0.006$

based on F^2, with a 3σ cut-off on F^2. A number of different multipole models were also tested, including refinement of the populations of higher multipoles up to hectoicosaoctopoles (128-poles), as well as the radial exponents of the multipoles. Although these parameters were sometimes stable in the least squares refinement, the values obtained were often accompanied by a large error (>3σ).

Despite the significant results obtained there were still substantial features in the residual maps, namely large positive and negative deformations around the antimony atom, which seemed unrealistically large. To solve these problems, analysis of model structure factors obtained from CRYSTAL98[21] was undertaken. Hartree–Fock level calculations were performed using Gaussian basis sets,[22] and the experimentally determined cell parameters and atomic positions from this study. A diffuse d-type function that caused convergence problems was removed from the antimony basis set, and the exponents of the most diffuse d and p valence functions on both atoms were optimised, and the final basis set has been deposited.[23] This

Table 2 Position and thermal parameters for senarmontite from the final multipole model[a]

	Sb	O
x	0.24017(1)	0.31182(9)
y	0.74017(1)	5/8
z	0.24017(1)	1/8
U_{11}	0.557(5)	0.76(3)
U_{22}	U_{11}	0.719(14)
U_{33}	U_{11}	U_{22}
U_{12}	U_{23}	–
U_{13}	U_{23}	–
U_{23}	−0.043(3);	−0.111(17)
C_{111};	−0.056(19)	–
C_{112};	−0.037(19)	–
C_{123}	0.32(5)	–
D_{1111}	0.0174(15)	–
D_{1112}	0.0000(15)	–
D_{1122}	0.018(3)	–
D_{1123}	0.000(2)	–

[a] U_{ij} are in units of 10^{-2} Å²; C_{ijk} and D_{ijkl} are dimensionless and have been multiplied by 10^5.

optimisation did not alter the appearance of the theoretical deformation density significantly, although greater charge accumulation at the rear of the antimony atom was observed. After the completion of this calculation a complete set of structure factors was generated to the resolution of the experimental data. These were analysed using VALRAY98,[18] initially in an analogous fashion to the analysis of the experimental data, with dispersion corrections and thermal parameters set to zero. After convergence of these initial refinements, multipole radial parameters were included, refining to values of 5.05 au for antimony and 5.77 au for oxygen. The resulting κ values for this refinement were 1.01 for antimony and 0.96 for oxygen, with corresponding charges of +1.13 for antimony and −0.75 for oxygen, derived from the sum over the monopole populations. When these radial parameters were applied to the experimental data and not refined, while all other parameters were refined, the unrealistically large peaks around the antimony atom disappeared. The κ values obtained for that refinement were 1.16(11) for antimony and 0.95(1) for oxygen, and the charges were +1.23(23) for Sb and −0.82(15) for O, in line with those obtained by multipole fitting of theoretical structure factors.[24]

Theoretical calculations were also performed on valentinite, using experimentally determined cell parameters and atomic positions from the X-ray data collected.[5] The basis sets used were the same as those described above.

Results and discussion

The crystal structure of senarmontite has been known since the early 20th century, and is readily found in monographs such as that by Wells.[25] Senarmontite consists of discrete Sb_4O_6 molecules having a crystallographically unique antimony site of $3m$ symmetry and an oxygen site with $mm2$ symmetry (Fig. 1). Each antimony defines the corner of a tetrahedron with Sb to Sb edge lengths of 3.6220(2) Å, and the oxygen atoms form corners of an octahedron with edge length 2.938(1) Å. The four antimony sites are centred 1.019(1) Å above four of the oxygen octahedron faces, such that the three metal to oxygen distances are 1.9784(6) Å. The antimony tetrahedra of adjacent molecules are arranged face to face such that the oxygen atoms linking the antimony atoms of one face are 2.9018(9) Å from the antimony of an opposing face. That is, each antimony is 1.9784(6) Å from three 'intramolecular' oxygen atoms and 2.9018(9) Å from the oxygen atoms for three adjacent Sb_4O_6 molecules. Within the molecular unit, the Sb–O–Sb bond angle is 132.51(7)° and the O–Sb–O angle is 95.87(5)°. Similar geometry is described in the most recent of the X-ray structural studies on senarmontite.[26]

Tetrahedral molecular units found in senarmontite crystals are known to exist in the gas phase with only a slight structural change from that observed in the crystal.[27] In the solid-state, these molecular units pack in a face-to-face, interlocking type arrangement as shown in Fig. 6. Other Group V elements such as phosphorus and arsenic also form oxides with the same molecular conformation as that displayed by senarmontite, and various X-ray[28] and electron diffraction[29] studies on these compounds have been published. These studies reveal that the bond angles are comparable to those of As_4O_6 in either the gas phase or solid state and to P_4O_6 in the gas phase.

In contrast to the molecular units present in senarmontite, valentinite is composed of "ladder-like" chains of Sb_2O_3 (Figs. 1 and 5) running parallel to the c axis of the orthorhombic unit cell. Each antimony has three oxygen 'coordination' contacts at 1.9835(9), 2.0242(6) and 2.0207(9) Å, and a lone pair of electrons completes a somewhat distorted tetrahedron about the antimony. In addition, there is a longer contact (2.6119(8) Å) between antimony and the oxygen defining the next 'rung' on the chain ladder (e.g. O(1c) in Fig. 1). The chains themselves are weakly linked together, with an 'inter-chain' metal to oxygen separation of 2.5070(9) Å. Additional geometric details are available in the CIF provided as electronic supplementary information, and are in accord with the most recent structural study.[4]

Deformation electron density maps are reported for senarmontite, obtained directly from theory (left of Fig. 2), and from
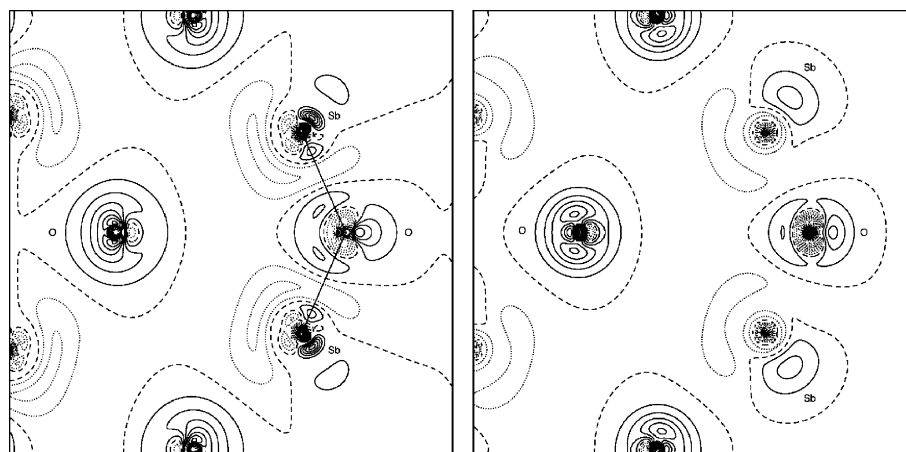

Fig. 2 Deformation electron densities for senarmontite: left: theoretical deformation electron density (CRYSTAL98[21]); right: model deformation density obtained from multipole fitting of CRYSTAL98 structure factors. Four atoms of a molecular Sb_4O_6 unit are in the (0 0 1) mapping planes, with the Sb–O–Sb moiety on the right, and the O atom on the left. Note that the sections through the symmetry-related O atoms are perpendicular to one another. The contour interval is 0.1 e Å⁻³.
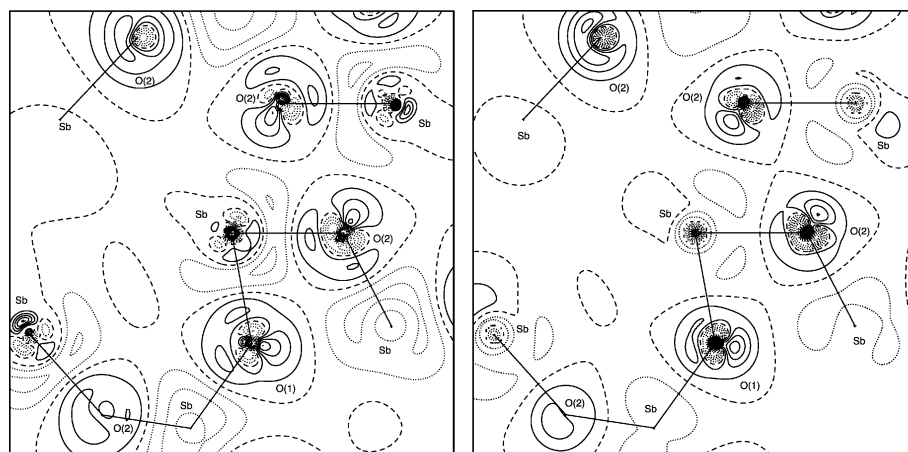
Fig. 3 Deformation electron densities for valentinite: left: theoretical deformation electron density (CRYSTAL98); right: model deformation density obtained from multipole fitting of CRYSTAL98 structure factors. The mapping plane is through Sb, O(1) and (2) and the contour interval is 0.1 e Å^{-3}.
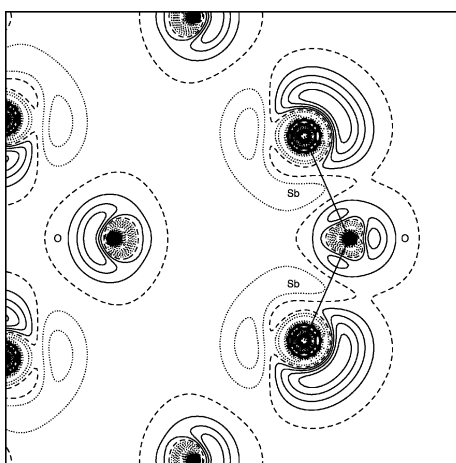

Fig. 4 Deformation electron density of senarmontite obtained from multipole fitting of experimental structure factors. The mapping plane and contour intervals are the same as in Fig. 2.

multipole fitting of theoretical (right of Fig. 2) and experimental (Fig. 4) structure factors. Although the correspondence between the three maps is not perfect, there are key features that are present in each case. The differences between the two maps in Fig. 2 are mainly due to the resolution of the generated structure factors that were fitted in the multipole refinement (the same as the experimental data, approximately 1.28 Å^{-1}). Fig. 2 (right) does not reveal the sharper features of the electron density around the antimony atom, which is not surprising, given that it was shown in a recent study on coesite[30] that very sharp features of the electron density are not present in the X-ray data below resolutions of about 1.8 Å^{-1}. If this finding is taken into account then it is clear that even with accurate data, discrepancies such as those observed in Fig. 2 must be expected. Comparison between theory and experiment is therefore best

made between Fig. 2 (right) and Fig. 4, and the correspondence between the two is actually quite good. Both maps show diffuse "lone pair" regions at the rear of the antimony atom (*i.e.* outside the Sb$_4$O$_6$ cage), and for oxygen there is an accumulation of charge outside the cage, and also in the "non-bonding" direction, perpendicular to the Sb–O–Sb bonds. The magnitudes of these deformations are also comparable between experiment and theory.

Fig. 3 compares deformation density maps of valentinite, obtained directly from theory (left) and from multipole fitting of theoretical structure factors (right). Comparison with Fig. 2 highlights the similar bonding present in both polymorphs; the shapes and magnitudes of the deformations of similar atoms are almost identical in the two compounds. Differences between features in the two maps in Fig. 3 are as observed for senarmontite in Fig. 2, and for the same reasons.

Topological analysis

Topological analysis of the theoretical densities was performed with TOPOND,[31] and those critical points were used as starting points for the critical point search in the experimental electron density of senarmontite, using VALRAY98.[18] Although only a necessary and not sufficient criterion for the location of all critical points, the Morse relation was satisfied for all experimental and theoretical densities. Positions of the critical points differed slightly between the experimental and theoretical electron densities for senarmontite, except for those lying on highly symmetric positions. The comparison between theoretical and experimental critical point preperties for senarmontite (Table 3) is uniformly excellent and within estimated experimental errors, which lends confidence when comparing results for valentinite (obtained directly from the theoretical calculation) with corresponding experimental or theoretical results for senarmontite. Although of lesser interest in the present study, the properties of the ring and cage critical points have also been included in
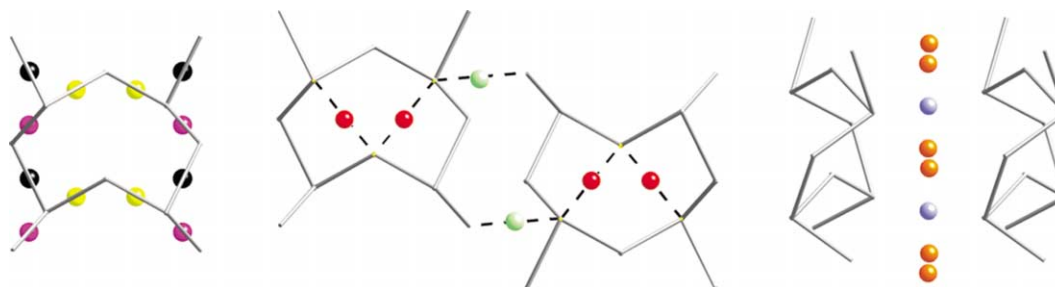

Fig. 5 The seven different (3, −1) bond critical points in valentinite. The left image shows those for close contacts between atoms in chains: light purple (*a*), black (*b*) and yellow (*c*). The central image shows medium length interactions, both between (light green (*d*)) and within (red (*e*)) chains. The right image corresponds to the longer interactions between chains: orange (*f*) and light blue (*g*). Properties of the bcps are given in Table 3.

Table 3 Theoretical critical point data for valentinite and senarmontite; values in italics are experimental results for senarmontite. The labels *a*, *b*, *c etc.* refer to the labelling of bcps in Figs. 5 and 6

	$\rho(\mathbf{r}_b)$/e Å^{-3}	$\nabla^2\rho(\mathbf{r}_b)$/e Å^{-5}	Distances to closest atoms/Å
Valentinite			
(3, +3)	0.016	0.182	–
(3, +3)	0.016	0.254	–
(3, +3)	0.013	0.241	–
(3, −1) *a*	0.747	11.735	Sb: 0.986; O(2): 0.998
(3, −1) *b*	0.688	10.482	Sb: 1.000; O(2): 1.020
(3, −1) *c*	0.670	10.533	Sb: 1.005; O(1): 1.019
(3, −1) *d*	0.239	2.890	O(2): 1.240; Sb: 1.276
(3, −1) *e*	0.195	2.421	O(1): 1.299; Sb: 1.321
(3, −1) *f*	0.056	0.389	Sb: 1.894, 2.038; O(2): 2.217
(3, −1) *g*	0.043	0.312	Sb: 2.068, 2.068
(3, +1)	0.154	2.615	–
(3, +1)	0.162	2.343	–
(3, +1)	0.144	2.276	–
(3, +1)	0.019	0.260	–
(3, +1)	0.043	0.596	–
(3, +1)	0.049	0.508	–
(3, +1)	0.022	0.266	–
Senarmontite			
(3, +3)	0.012	0.289	–
	0.017(5)	*0.22(3)*	–
(3, +3)	0.024	0.441	–
	0.033(13)	*0.32(8)*	–
(3, +3)	0.015	0.181	–
	0.007(4)	*0.087(22)*	–
(3, +3)	0.004	0.063	–
	0.004(2)	*0.045(17)*	–
(3, −1) *h*	0.742	11.953	0.987 (Sb), 0.992 (O)
	0.66(4)	*13.1(12)*	*0.954 (O), 1.029 (Sb)*
(3, −1) *i*	0.120	1.294	1.403 (O), 1.511 (Sb)
	0.116(16)	*1.37(9)*	*1.356 (O), 1.563 (Sb)*
(3, +1)	0.088	1.280	–
	0.079(12)	*1.04(5)*	–
(3, +1)	0.053	0.868	–
	0.051(13)	*0.57(7)*	–
(3, +1)	0.019	0.205	–
	0.010(5)	*0.122(22)*	–

Table 4 Theoretical energy density quantities for valentinite and senarmontite; values in italics are experimental results for senarmontite. The labels *a*, *b*, *c etc.* refer to the labelling of bcps in Figs. 5 and 6

	$G(\mathbf{r}_b)$/E_h Å^{-3}	$V(\mathbf{r}_b)$/E_h Å^{-3}	$H(\mathbf{r}_b)$/E_h Å^{-3}
Valentinite			
a	1.071	−1.320	−0.249
b	0.952	−1.170	−0.218
c	0.942	−1.146	−0.204
d	0.217	−0.232	−0.015
e	0.174	−0.179	−0.005
f	0.025	−0.022	0.003
g	0.019	−0.019	0.003
Senarmontite			
h	1.078	−1.317	−0.239
	1.02(7)	*−1.12(9)*	*−0.10(5)*
i	0.087	−0.085	0.003
	0.086(7)	*−0.076(7)*	*0.010(6)*

between Sb and O atoms, and these can be identified as intramolecular and intermolecular bonds. Earlier it was mentioned how the molecular units in senarmontite pack in an interlocking arrangement, with weak intermolecular bonds expected between oxygen and antimony atoms directly opposite each other. The location of bond critical points between oxygen and antimony atoms within (*h*) and between (*i*) different molecular units verifies the existence of the expected interactions (Fig. 6). The six-coordinate nature of the antimony atom and the four-coordinate nature of the oxygen atom are also evident when taking these intermolecular bcps into account.
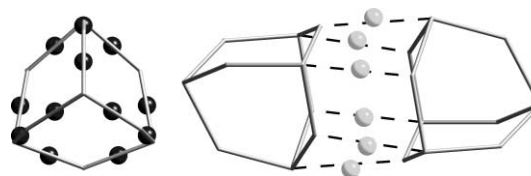

Fig. 6 The two (3, −1) bond critical points in senarmontite. Each image portrays the face of a molecular Sb_4O_6 unit in relation to the intramolecular (dark gray (*h*); left) and intermolecular (light gray (*i*); right) critical points. Properties of the bcps are given in Table 3.

Table 3, and from them it can be seen that the reconstruction of the total electron density in the crystal is uniformly excellent, not only in the vicinity of bonding interactions, but also where the electron density is more diffuse. The remaining discussion in this section will focus on a quantitative analysis of the bond critical points (bcps).

The bonding arrangement in valentinite is the more complicated of the two polymorphs (Fig. 5). As expected, there are three different close contacts (*a*, *b* and *c*), and two slightly longer interactions, one within a given polymer chain (*e*) and one between polymer chains (*d*), all revealed by the existence of bcps and bond paths between Sb and O atoms (Table 3). In addition, there are two very long interactions, *f* and *g*. The shorter of these (*f*) could be classified as a longe range interaction between O(2) and antimony atoms in different chains, but in fact the closest two atoms to this bcp are both Sb atoms. The longest contact in valentinite (*g*) lies on a two-fold axis, and the closest atoms to this bcp are two Sb atoms at 2.068 Å. Clearly these longest interactions in valentinite are not only weak, as characterised by values of the electron density and Laplacian, but they result from long-range Sb · · · Sb interactions rather than Sb · · · O interactions. We conclude that in valentinite each Sb atom is essentially five-coordinate, while O(1) is four-coordinate and O(2) is three-coordinate.

Senarmontite exhibits two different interatomic contacts, *h* and *i*, both identified by the presence of a bcp and bond paths

As stated in the Introduction, a key motivation behind this work was the expectation that quantitative information regarding the bonding in these two polymorphs might provide insight into their differing reactivities. In recent years there have been many attempts to characterize interatomic interactions in terms of properties of the bcps, and these typically rely on classifications originally proposed by Bader and Essén[32] or by Cremer and Kraka,[33] and use values of $\rho(\mathbf{r}_b)$, $\nabla^2\rho(\mathbf{r}_b)$ and its components, and the relative magnitudes of the local kinetic, $G(\mathbf{r}_b)$, potential, $V(\mathbf{r}_b)$, and total, $H(\mathbf{r}_b)$, energy densities. For the present purposes we note that although more recent classifications have been proposed in attempts to encompass all bond types,[34] and some very comprehensive analyses have been made of hydrogen bonding interactions,[35] we base our comments on work by Gibbs *et al.*,[36] who studied a wide range of bonds involving oxygen atoms. Gibbs *et al.* relied largely on values of $\rho(\mathbf{r}_b)$, $\nabla^2\rho(\mathbf{r}_b)$ and $H(\mathbf{r}_b)$, and in particular found that the total energy density, $H(\mathbf{r}_b)$, was crucial in their analyses. The equations presented by Abramov[37] have been used to compute experimental local energy density quantities at the bcps in senarmontite (Table 4), and these are generally comparable with those calculated directly from theory, especially allowing for the estimated errors propagated from experimental errors in the multipole model. Applying the considerations by Gibbs *et al.*[36] to the present bcp data enables connections to be made between the bonding in the two polymorphs, and the
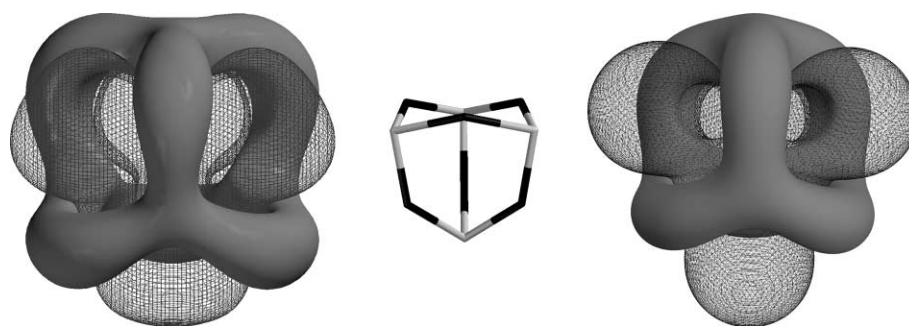
Fig. 7 Electrostatic potential isosurfaces for a molecular Sb_4O_6 unit in senarmontite. Left: *ab initio* result from SPARTAN using a DN* basis set; right: experimental result from multipole fitting procedure. In both cases the mesh isosurface is at 0.04 e Å^{-1}, and the solid isosurface at -0.04 e Å^{-1}. Molecular orientation is identical for both maps, and indicated in the molecular diagram at the centre (antimony atoms grey, oxygen atoms black).

easiest comparison is between the theoretical results (*i.e.* obtained directly from CRYSTAL98 [21]).

Properties for the nine bcps in these two polymorphs allow ready classification into four bond types, in the following manner:

(i) $\nabla^2\rho(r_b)$ ~10–12 e Å^{-5}, $\rho(r_b)$ ~0.7 e Å^{-3}, $H(r_b)$ ~-0.20 to -0.25 E_h Å^{-3}, corresponding to normal polar covalent Sb–O interactions, very similar to those observed for Si–O and Ge–O, and includes bcps for all four close contacts: *a*, *b*, *c* and *h*.

(ii) $\nabla^2\rho(r_b)$ ~2.4–3.0 e Å^{-5}, $\rho(r_b)$ ~0.2 e Å^{-3}, $H(r_b)$ very small and negative, corresponding to either very weak polar covalent, or closed-shell Sb $\cdots$ O interactions, and includes the intra- and inter-chain bcps in valentinite: *d* and *e*.

(iii) $\nabla^2\rho(r_b)$ ~1.0 e Å^{-5}, $\rho(r_b)$ ~0.1 e Å^{-3}, $H(r_b)$ very small and positive, corresponding to weaker closed-shell Sb $\cdots$ O interactions, specifically the intermolecular bcp in senarmontite, *i*.

(iv) $\nabla^2\rho(r_b)$ <0.5 e Å^{-5}, $\rho(r_b)$ ~0.05 e Å^{-3}, $H(r_b)$ very small and positive, corresponding to very weak closed-shell Sb $\cdots$ Sb interactions: *f* and *g*.

In this manner we see that the shortest contact in valentinite is very similar to the short contact in senarmontite (compare results for *a* and *h* in Tables 3 and 4), in both topology and length, while the other two close contacts in valentinite (*b* and *c*) are almost identical to each other and are not too far removed in nature from *a* and *h*. The longer atom–atom contacts in these two compounds show greater variation. In valentinite the bcps of the two longer contacts (*d* and *e*) display considerably more electron density at the bcp than does *i* in senarmontite, and are also substantially shorter (by approximately 0.2 Å). Even between *d* and *e* there is large variation, *d* being the stronger interaction, holding chains together, while *e* is a weaker interaction, dictating more the shape of the chains, rather than binding the chains together. The remaining bcps (*f* and *g*) are classified as bonding interactions, but they are extremely weak.

Electrostatic potential

The electrostatic potential is an important property that can be derived from the electron density, and gives an indication of where reactants will be first attracted during a reaction, information that may be valuable at a later stage of this study. Fig. 7 displays two isosurfaces of the electrostatic potential for an isolated Sb_4O_6 unit in the senarmontite structure. The image on the left is from a perturbative DFT (pBP) calculation using a double numerical DN* basis set in SPARTAN,[38] on a single molecule possessing the same geometry as that observed in the solid state, while the image on the right is based on the multipole-derived experimental electron density distribution. There is obvious agreement between experiment and theory in these two figures. Simple electronegativity arguments would predict regions of negative potential around the oxygen atoms and regions of positive potential around antimony, but the enveloping band of negative potential (the solid surface) observed in both figures is surprising, and quite striking. Clearly the

substantial "non-bonding" deformations observed in Figs. 2 and 4 about the O atoms, and perpendicular to the Sb–O–Sb plane, have a significant and far-reaching effect on the electrostatic potential outside the molecule. The general topology of the positive and negative isosurfaces in Fig. 7 also makes it clear why these molecular units pack face to face as they do in the crystal (Fig. 6), with regions of negative potential in one molecule overlapping with regions of positive potential in a neighboring molecule.

Conclusions

Despite a number of difficulties, X-ray data of reasonable quality can be collected on compounds containing quite heavy atoms, such as antimony oxides, for the purposes of topological analysis of the electron density.[39] This study presented theoretical results for both senarmontite and valentinite, but only experimental results for senarmontite as poor crystal quality compromised the X-ray data for the other polymorph. Nevertheless, definitive conclusions were made about the nature of the bonding interactions in these materials, and a comparison could be made between the two polymorphs. The closest interatomic interactions are polar covalent in nature, and the weaker intermolecular and interchain contacts are of closed-shell type. Valentinite also shows evidence of two very weak and long Sb $\cdots$ Sb interactions between polymeric chains. Electrostatic potential isosurface maps reveal the marked octopolar nature of this function for senarmontite, and aid in understanding the packing arrangement of Sb_4O_6 molecules in the crystal.

Acknowledgements

References

1 T. Lippmann, P. Blaha, N. H. Andersen, H. F. Poulsen, T. Wolf, J. R. Schneider and K. Schwarz, *Acta Crystallogr., Sect. A*, 2003, **59**, 437; A. Kirfel, H.-G. Krane, P. Blaha, K. Schwarz and T. Lippmann, *Acta Crystallogr., Sect. A*, 2001, **57**, 663; T. Lippmann and J. R. Schneider, *J. Appl. Crystallogr.*, 2000, **33**, 156; T. Lippmann and J. R. Schneider, *Acta Crystallogr., Sect. A*, 2000, **56**, 575.

2 R. F. W. Bader, *Atoms in Molecules – a Quantum Theory*, Oxford University Press, Oxford, 1990.

3 M. A. Spackman, *Annu. Rep. Prog. Chem., Sect. C: Phys. Chem.*, 1997, **94**, 177.

4 C. Svensson, *Acta Crystallogr., Sect. B*, 1974, **30**, 458; C. Wood, B. van Pelt and A. Dwight, *Phys. Status Solidi B*, 1972, **54**, 701.

5 In the sublimation vessel, both valentinite and senarmontite formed. Diffraction data on valentinite (*Pccn*) was also collected in the same manner as described for senarmontite, but the crystal shape was anomalous and the analytical absorption correction did not model

the effect well. Hence multipole refinements reconstructed the electron density distribution poorly. The relevant structural parameters obtained from a spherical atom refinement are: a = 4.8996(3) Å, b = 12.4490(7) Å, c = 5.4103(3) Å, $\alpha = \beta = \gamma = 90°$. Sb (0.04064, 0.12753, 0.17784), O(1) (1/4, 1/4, 0.0209), O(2) (0.1509, 0.0587, −0.1454). Full crystallographic details are included in the CIF file.

6 SMART, SAINT, ASTRO and XPREP: Data Collection and Processing Software for the SMART System, Bruker, Madison, WI, 1995.
7 R. H. Blessing, *J. Appl. Crystallogr.*, 1997, **30**, 421.
8 teXsan for Windows: Single crystal structure analysis software, Molecular Structure Corporation, The Woodlands, TX, 1997–1998.
9 L. J. Farrugia, *J. Appl. Crystallogr.*, 1999, **32**, 837.
10 XSHELL, Graphical interface for crystal structure refinement, Bruker, Madison, WI, 1995.
11 G. M. Sheldrick, SHELXS-97, Program for solution of crystal structures, University of Göttingen, Germany, 1997.
12 G. M. Sheldrick, SHELXL-97, Program for refinement of crystal structures, University of Göttingen, Germany, 1997.
13 C. K. Johnson, ORTEPII. Report ORNL-5138. Oak Ridge National Laboratory, Oak Ridge, TN, 1976; Xtal3.6 System, ed. S. R. Hall, D. J. du Boulay and R. Olthof-Hazekamp, University of Western Australia, 1999.
14 E. Clementi and C. Roetti, *At. Data Nucl. Data Tables*, 1974, **14**, 177.
15 D. C. Creagh, and W. J. McAuley, Section 4.2.6 in *International Tables for Crystallography, Volume C: Mathematical, Physical & Chemical Tables*, Kluwer, Dordrecht, 1995.
16 P. Coppens, *X-Ray Charge Densities and Chemical Bonding*, Oxford University Press, Oxford, 1997.
17 C. Flensburg, S. Larsen and R. F. Stewart, *J. Phys. Chem.*, 1995, **99**, 10130.
18 R. F. Stewart, M. A. Spackman and C. Flensburg, VALRAY98 Users Manual, Carnegie Mellon University & University of Copenhagen, 1998.
19 The coordinate system defined for the multipoles was: x = (1,0,0) and y = (0,1,0). For this coordinate system, the multipole constraints used were: Sb, $Y_{11+} = Y_{11-} = Y_{10}$, $Y_{22-} = Y_{21+} = Y_{21-}$, $Y_{33+} = -Y_{33-} = -5/3\,Y_{31+} = -5/3\,Y_{31-} = 5/4\,Y_{30}$), Y_{32-} was refined unconstrained. O, $Y_{22+} = -Y_{20}$, $Y_{33+} = -5/3\,Y_{31+}$, Y_{11+}, Y_{21-} and Y_{32-} were refined unconstrained.
20 P. J. Becker and P. Coppens, *Acta Crystallogr., Sect. A*, 1974, **30**, 129.
21 V. R. Saunders, R. Dovesi, C. Roetti, M. Causa, N. M. Harrison, R. Orlando and C. M. Zicovich-Wilson, CRYSTAL98 User's Manual, University of Torino, Torino, 1998.
22 N. Godbout, D. R. Salahub, J. Andzelm and E. Wimmer, *Can. J. Chem.*, 1992, **70**, 560.
23 M. D. Towler, Billy – Basis set optimisation script for CRYSTAL98 calculations, University of Cambridge, UK, 2000; M. D. Towler, CRYSTAL98 Resource page: (http://www.tcm.phy.cam.ac.uk/~mdt26/crystal.html), 2001.
24 In comparison, Mulliken charges obtained from the CRYSTAL98 calculations are somewhat greater: for senarmontite, +1.76 on Sb, and −1.17 on O, and for valentinite, +1.77 on Sb, −1.23 on O(1) and −1.15 on O(2).
25 A. F. Wells, *Structural Inorganic Chemistry*, Clarendon Press, Oxford, 5th edn., 1984.
26 C. Svensson, *Acta Crystallogr., Sect. B*, 1975, **31**, 2016.
27 P. A. Ashkin and V. P. Spiridonov, *Zh. Strukt. Khim.*, 1961, **2**, 542.
28 R. M. Bozorth, *J. Am. Chem. Soc.*, 1923, **45**, 1621.
29 P. A. Ashkin and V. P. Spiridonov, *Zh. Strukt. Khim.*, 1961, **2**, 542; B. Beagly, D. W. J. Cruickshank, T. G. Hewitt and K. H. Jost, *Trans. Faraday Soc.*, 1969, **65**, 1219; C. S. Lu and J. Donohue, *J. Am. Chem. Soc.*, 1944, **66**, 818.
30 G. V. Gibbs, A. E. Whitten, M. A. Spackman, M. Stimpf, R. T. Downs and M. D. Carducci, *J. Phys. Chem. B*, 2003, **107**, 12996.
31 C. Gatti, TOPOND-98 Users Manual, CNR-CSRSRC, Milano, 1999.
32 R. F. W. Bader and H. Essén, *J. Chem. Phys.*, 1984, **80**, 1943.
33 D. Cremer and E. Kraka, *Croat. Chim. Acta*, 1984, **57**, 1259.
34 See, for example: P. Macchi, D. M. Proserpio and A. Sironi, *J. Am. Chem. Soc.*, 1998, **120**, 13429; R. Bianchi, G. Gervasio and D. Marabello, *Inorg. Chem.*, 2000, **39**, 2360.
35 See E. Espinosa, I. Alkorta, J. Elguero and E. Molins, *J. Chem. Phys.*, 2002, **117**, 5529, and references therein.
36 F. C. Hill, G. V. Gibbs and M. B. Boisen, *Phys. Chem. Mineral.*, 1997, **24**, 582; G. V. Gibbs, M. B. Boisen, F. C. Hill, O. Tamada and R. T. Downs, *Phys. Chem. Mineral.*, 1998, **25**, 574.
37 Y. A. Abramov, *Acta Crystallogr., Sect. A*, 1997, **53**, 264.
38 SPARTAN version 5.0, Wavefunction Inc., 18401 Von Karman Ave., Irvine CA 92715, USA. The DN* basis set is slightly larger than the common 6-31G* basis set.
39 We note that in this study, and most likely other studies involving heavy atoms, proper treatment of absorption is vital, and in some cases it may be a greater problem than extinction. For senarmontite, if the most heavily extinction-affected reflections were removed from the refinement very little changed, but small optimisations made to the crystal dimensions, subsequently used in the absorption correction, substantially altered the deformation density and derived properties.